A SOLAR FLARE OBSERVED WITH THE SMM AND *EINSTEIN* SATELLITES

J. H. M. M. SCHMITT

Max-Planck-Institut für extraterrestrische Physik, 8046 Garching, F.R.G.

J. R. LEMEN

Lockheed Palo Alto Research Laboratories, U.S.A.

and

D. ZARRO

Applied Research Corporation at NASA/GSFC, U.S.A.

Abstract. We present X-ray observations of the 21 July, 1980 flare which was observed both with the *Einstein* Observatory Imaging Proportional Counter (IPC) and the X-Ray Polychromator (XRP) and Gamma-Ray Spectrometer onboard the SMM satellite. The *Einstein* observations were obtained in scattered X-ray light, i.e., in X-rays scattered off the Earth's atmosphere. In this way it is possible to obtain spatially unresolved X-ray data of a solar flare with the same instrument that observed many X-ray flares on other stars. This paper juxtaposes the results and implications of the 'stellar interpretation' to those obtained from the far more detailed SMM observations. The result of this 'calibration' observation is that the basic properties of the flaring plasma can be reliably determined from the 'stellar' data, however, the basic physics issues can only be studied through models.

1. Introduction

Imaging soft X-ray telescopes such as flown onboard the *Einstein* and EXOSAT satellites have provided a large number of observational examples of stellar X-ray flares (Haisch, 1983; Pallavicini, 1987; Collura, Pasquini, and Schmitt, 1988; Pallavicini and Schmitt, 1988). Flares are observed not only on the previously known (optical) flare stars, i.e., on late-type M dwarf stars, but also on RS CVn systems, solar-like stars and possibly even on A-type stars (Pallavicini *et al.*, 1989). On the Sun the occurrence of flares is, of course, quite a common phenomenon and flares have been the object of study of a concert of dedicated instruments flown onboard Skylab and SMM. In particular, the SMM satellite allowed simultaneous monitoring of solar flares from γ-rays to soft X-rays with very high time resolution. At soft X-ray energies, spectral resolution of $\lambda/\Delta\lambda \sim 10000$ could be accomplished, allowing the measurement of line profiles and Doppler shifts; further, spatial resolution of ~ 15 arc sec was possible up to photon energies of ~ 10 keV. The wealth and detail of the SMM observations greatly advanced our understanding of the physical processes occurring in solar flares.

The data quality of stellar X-ray observations is of course far inferior to that obtained with state-of-the-art observations of the Sun in every respect. First of all, spatial resolution is totally absent and, hence, no direct information on the size of the emitting regions is available. Second, the stellar X-ray observations are typically carried out at lower energy (in the pass band 0.2–4.0 keV with the *Einstein* Observatory and

Solar Physics **121:** 361–373, 1989.

0.04–2.0 keV with the EXOSAT LE), and little or no sensitivity remains at higher energies; in particular, no information is available on non-thermal X-ray emission and further, the energy resolution of the soft X-ray data is very limited ($\Delta E/E \sim 1$) for the *Einstein* Observatory IPC or absent (for the EXOSAT LE). Lastly, the time resolution of stellar flare observations is far worse than that of solar observations due to counting statistics; although the X-ray observations are typically carried out in photon counting mode with the arrival times of individual photons measured with an accuracy of a few milliseconds or better, the count rates of the observed stellar flare events are typically rather low (say, 0.1–1 counts s^{-1}), and, therefore, it is difficult to detect variability on time scales less than ~ 1 min in a statistically significant way.

Consequently, the basic X-ray observations of a stellar flare consist of a light curve (possibly in various energy bands) and thus an estimate of a decay time, a flux (implying an emission measure) and possibly a rather coarse estimate of X-ray temperature obtained from fitting theoretical model spectra to broad-band X-ray data (cf. Pallavicini *et al.*, 1987). The inference of the physical parameters of the flaring plasma (such as temperature, size, and density of the flaring region) on a star must, therefore, be rather indirect and in particular involves assumptions on the relevant cooling time scales. Using such indirect arguments one typically finds stellar flares to be far more energetic than their solar counterparts; however, the sizes of the flaring regions are almost always found to be small compared to the stellar radius, implying the presence of rather dense and hot material in the coronae of stars.

Schmitt, Harnden, and Fink (1987) report X-ray observations of solar flares with the *Einstein* Observatory. While this telescope was designed exclusively for non-solar cosmic X-ray observations and could, therefore, not be pointed directly at the Sun, solar X-rays scattered off the Earth's atmosphere were recorded while the Sun-lit Earth intercepted the telescope's field-of-view. By modelling the propagation of solar X-rays in the Earth's atmosphere (see Fink, Schmitt, and Harnden, 1988 for details) it is possible to disentangle variations in the observed scattered X-ray flux due to the continuously changing viewing geometry from intrinsic variations in the incident solar X-ray flux. Thus an X-ray light curve of a solar flare can be obtained which has – since obtained with the same instrument – all the observational attributes of a stellar flare observation. The purpose of this paper is to present and discuss the SMM observations of the same flare, to compare the parameters derived from the stellar modelling of the July 21, 1980 flare to the direct measurements obtained with the SMM satellite, and to investigate how much of the physics of stellar flares can be deduced from the available soft X-ray observations.

2. The *Einstein* Observations of the Flare on July 21, 1980

A detailed description of the *Einstein* observations of scattered solar X-rays was given by Schmitt, Harnden, and Fink (1987; hereafter abbreviated as SHF) and Fink, Schmitt, and Harnden (1988; abbreviated as FSH); here we only summarize the most important issues and refer those readers interested in the detailed modelling to the above papers.

When the X-ray telescope is pointed at the Sun-lit Earth, solar X-ray photons scatter off the atoms and molecules of the Earth's atmosphere, enter the telescope aperture and form a diffuse 'image' of the Sun in the detector plane. Depending on the photon energy, either Thomson scattering or fluorescent scattering predominates, however in the so-called carbon window between 0.2 and 0.28 keV where the IPC is most sensitive all photons are Thomson scattered. In both cases, however, the ratio between scattering and absorption cross section is small, so that for a theoretical description of photon propagation at X-ray energies in the Earth's atmosphere a single-scattering description suffices. Due to the inherent three-dimensional nature of the problem this simplifies the radiative transfer calculations enormously; in planar geometry which approximately applies under certain viewing conditions the problem can be solved analytically.

FSH showed that the X-ray light curves of *Einstein* Observatory bright Earth passes can be satisfactorily modelled under a variety of viewing conditions assuming the incident solar flux to be constant. SHF reported three bright Earth passes which could not be modelled under the constant flux assumption and argued that the modelling procedure failed because of the occurrence of solar flares. The event which was by far the strongest among those reported by SHF was the flare on July 21, 1980, commencing at 2:56 UT.

In the upper panel of Figure 1 we show the observed IPC light curve during the bright Earth pass; the smooth curve shows the best model fit to the data and the lower

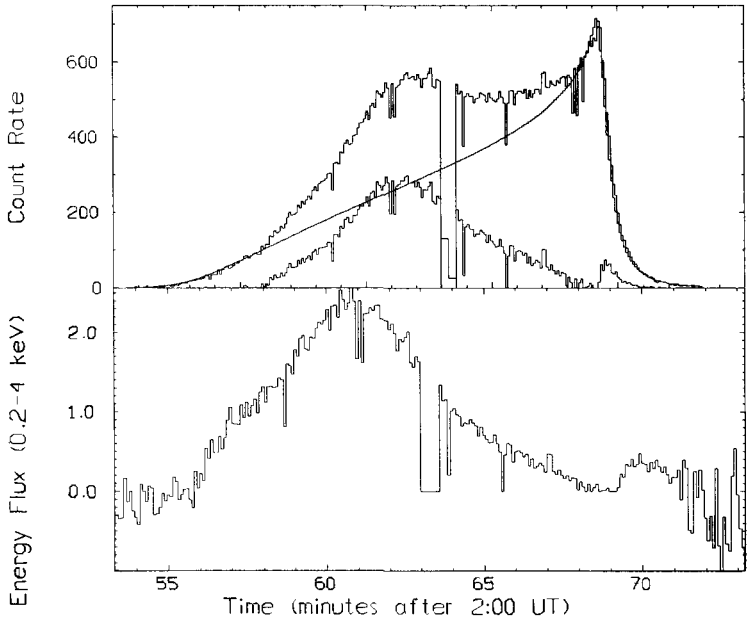

Fig. 1a–b. (a) Observed IPC light curve (upper histogram) as function of time; the smooth curve represents the best fit assuming constant incident flux, the bottom curve is the residual attributed to the flare, containing both intrinsic as well as geometric variations. (b) Inferred energy flux in the IPC flare as a function of time.

https://doi.org/10.1017/S0252921100031997 Published online by Cambridge University Press

histogram shows the excess count rate attributed to the flare. Note that this histogram still contains contributions from geometric variability as well as intrinsic flux variations.

Our model fits to the data have significantly improved compared to the method used by SHF and FSH. In particular, instead of a monochromatic calculation we now use an empirical solar X-ray spectrum for the quiet and flaring Sun (extracted from Manson, 1976) to compute the scattered solar X-ray flux. This procedure removes the difficulty encountered by SHF and FSH of having to fix the flux scattered through Thomson and fluorescent scattering and allows an immediate computation of the energy flux measured by direct observation of the Sun. This inferred energy flux in the IPC pass band is plotted in the lower panel of Figure 1. Flare onset occurs at about 2:55:40 UT with the peak count rate occurring at about 3:00:40 UT. The rise to maximum is not linear but has an inflection point at 2:58:20 UT. At flare maximum a flux of ~ 2.4 erg s^{-1} cm^{-2} is inferred; it should, however, be kept in mind that the energy fluxes inferred from the broad band data are probably no better than $\sim 50\%$. (Note that an IPC count rate of $\sim 3 \times 10^{11}$ counts s^{-1} would have been expected had the instrument been pointed at the Sun!).

In Table I, extracted from SHF, we summarise the physical parameters of the flare of July 21, 1980 as derived from the IPC observations. Clearly, the bright earth data offer an excellent opportunity to compare full disk IPC observations of solar flares to full disk IPC observations of stellar flares. The IPC measurements clearly show the soft X-ray emitting flare plasma heat and cool; further, the derived parameters are consistent with the properties of compact loop flares, the most commonly type of flare found on the Sun. Specifically, the IPC data indicate peak temperatures of the flare plasma of $\log T \sim 7.25$; and second, characteristic length scales of $\sim 3 \times 10^9$ cm. We re-emphasise that both of these findings were obtained with broad band data having no spatial resolution. In the following we want to examine to what extent the SMM data support this picture.

3. The SMM Observations of the Flare on July 21, 1980

The Solar Maximum Mission (SMM) spacecraft was launched on February 14, 1980, being operational through November 1980 before its repair in April 1984. SMM observed the flare on July 21, 1980 with both the X-ray Polychromator (XRP) and the Gamma-Ray Spectrometer (GRS); HXIS imaging data at higher energies are unfortunately not available for this flare.

3.1. The XRP data

3.1.1. *The Instrument*

A detailed description of the XRP is given by Acton *et al.* (1980). Briefly the XRP consists of a Flat Crystal Spectrometer (FCS) and a Bent Crystal Spectrometer (BCS). The BCS can be used for high resolution ($\lambda/\Delta\lambda \sim 10000$) X-ray spectroscopy in the wavelength range between ~ 1.8 and 2.5 Å, in particular it can study the dielectronic satellite spectra of the helium-like ions Ca XIX and Fe XXV which are rich in diagnostic

https://doi.org/10.1017/S0252921100031997 Published online by Cambridge University Press

applications; the BCS collimator field of view is 6 arc min with no imaging capability. The crystals of the FCS are rotatable and, therefore, cover a rather wide spectral range between ~1.4–22.4 Å, in addition, by rastering spectroheliograms with an angular resolution of ~14 arc sec can be obtained in the resonance lines of O VIII, Ne IX, Mg XI, Si XIII, Su XV, and Fe XXV.

For the flare on July 21, 1980 a complete BCS light curve in the lines of Ca XIX and Fe XXV is available. The FCS was used for rastering in the rise time of the flare (i.e., from 2:54 to 03:02 UT); afterwards, i.e., from 3:02 to 3:14 UT an X-ray light curve of the brightest spot in the previously obtained X-ray image in the lines of O VIII, Ne IX, Mg XI, Si XIII, Su XV, and Fe XXV is available. In the following sections we shall describe these data in detail.

3.1.2. *The BCS Observations*

In Figure 2 the Ca XIX and Fe XXV light curves as recorded by the BCS are shown. Flare onset occurs slightly before 2:55 UT, with the count rate first rather smoothly increasing, followed by a rapid increase between 2:56–2:57:30 UT. The Ca XIX count rate stays approximately constant, and the Fe XXV count rate decreases slightly before another rapid increase in count rate starts at 2:59 UT. Flare maximum is reached at 3:00 UT followed by a swift decay in count rate to preflare levels in about 5 min.

A comparison between the BCS light curves in Ca XIX and Fe XXV (see Figure 2) and the IPC light curve (Figure 1) reveals a striking similarity. Flare onset in the IPC occurs a little later; note, however, that the beginning of the flare depends sensitively on the subtraction procedure, hence, the difference is not significant. A break in the rising part

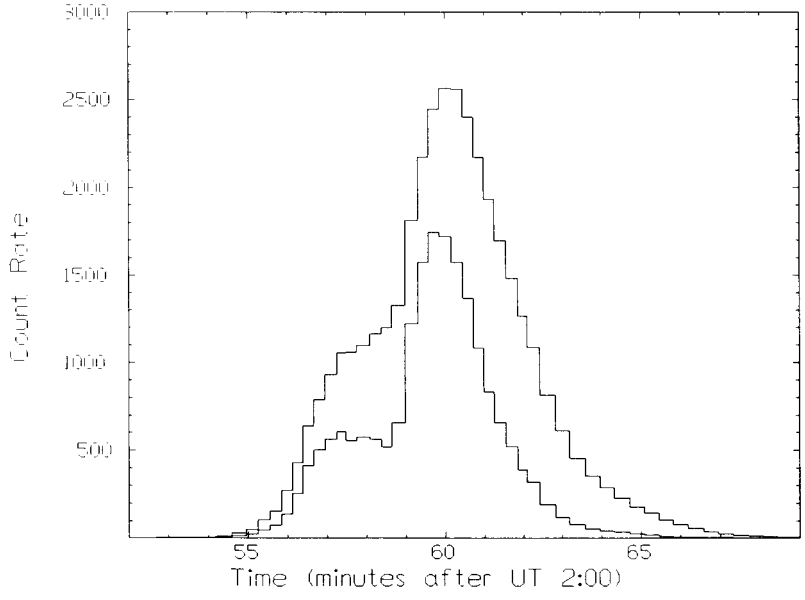

Fig. 2. BCS light curves in the Ca XIX (upper curve) and Fe XXV (lower curve) lines.

https://doi.org/10.1017/S0252921100031997 Published online by Cambridge University Press

of the flare at 2:57:30 UT is visible; the flare maximum is reached at the same time. The decay time-scale of the IPC light curve seems to be somewhat larger; this is of course not surprising since the IPC is more sensitive to lower temperature material and has little or no sensitivity at the Ca XIX and Fe XXV wavelengths, respectively. At any rate, the correctness of the interpretation of the IPC data obtained by SHF without knowledge of the SMM data is beyond any doubt.

For purposes of comparison to the broadband fluxes measured with the IPC one needs to know the run of temperature and emission measure with time, which are plotted in Figures 3(a) and 3(b) as derived from the Ca XIX and Fe XXV data respectively. The

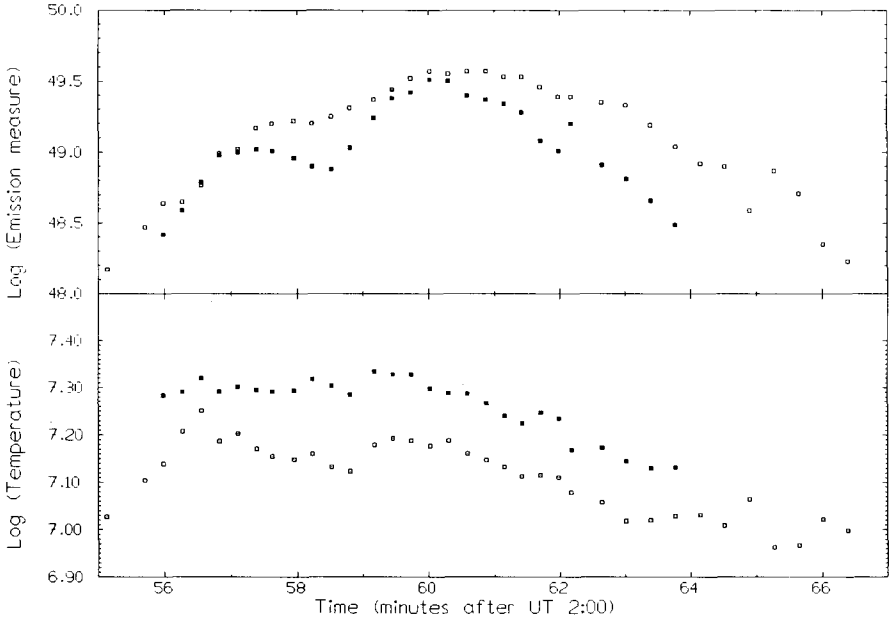

Fig. 3. (Logarithmic) temperature (*lower panel*) and emission measure (*upper panel*) derived from the Ca XIX (open squares) and Fe XXV (solid squares) data as a function of time.

theory of dielectronic recombination spectra and the problems of derivations of physical parameters from such spectra are extensively discussed in the literature (see, for example, Gabriel, 1972; Antonucci *et al.*, 1982; Lemen *et al.*, 1984). Note that the BCS emission measures have not been corrected for the collimator response which amounts to a factor of ~ 2 since the flare occurred close to the edge of the field of view as shown by the FCS raster images. As is evident from Figure 3 temperatures and emission measures derived from different lines do not agree, an effect attributed to the heterothermal nature of the emitting plasma (see Strong *et al.*, 1986).

In summary, the BCS spectra and light curve show a temperature stratification of the hot thermal flare plasma. The emission measure derived for the Ca XIX and Fe XXV evolve differently with time, the Fe XXV light curve hints at a second episode of energy input after an initial energy release.

https://doi.org/10.1017/S0252921100031997 Published online by Cambridge University Press

3.1.3. *The FCS Observations*

FCS images of the active region 2562 were taken on July 21, 1980 starting at 2:53 UT, i.e., in the rising phase of the flare, at 3:13 UT, i.e., immediately after the end of the flare, and at 3:34 UT. As an example we show (in Figure 4) a contour plot of the O VIII raster image taken between 2:53 and 3:02 UT. In this line (as well as in the images

Fig. 4. Contour plot of the O VIII FCS raster image taken between 02:54 and 03:02 on July 21, 1980; note the diffuse emission from active region 2562 as well as the flare in the lower right hand part.

in the lines of Ne IX and Mg XI) a region of diffuse emission is definitely visible during and after the flare, presumably part of the loop system of the active region 2562. The flare itself is clearly visible in all FCS images taken in the time interval 2:53–3:02 UT. At higher energies the flaring region becomes less pronounced, and in Si XIII and S XV virtually no excess emission is seen later than 3:13 UT.

In the lines of Si XIII and S XV the flare is unresolved, whereas in the lower temperature lines the flare may be resolved; this is, however, difficult to ascertain since the flare is located on top of an area with diffuse emission (cf. Figure 4). We, therefore, adopt as angular size of the flaring region $\theta \leq 14''$, the pixel size of the FCS, which translates into $L \leq 10^9$ cm. Therefore, the FCS images demonstrate directly the compact nature of the event on July 21, 1980.

Between 3:02 and 3:13 UT a light curve of the brightest spot in the FCS image is available in each spectral line. This brightest spot is likely to contain most of the flaring region; problems would however arise if the flaring region moved with respect to the instrument during FCS data taking. Figure 5 shows the FCS light curves in the lines of O VIII, Ne IX, Mg XI, Si XIII, and S XV, respectively. At higher temperatures no significant emission is found later than 3:06 UT, very much in line with the BCS Ca XIX

https://doi.org/10.1017/S0252921100031997 Published online by Cambridge University Press

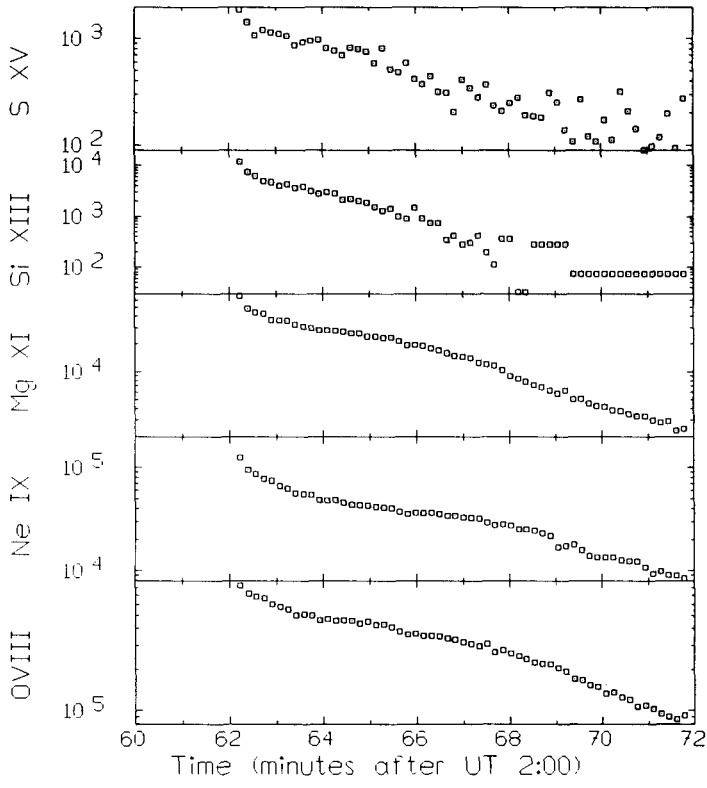

Fig. 5. FCS light curves in the O VIII, Ne IX, Mg XI, Si XIII, and S XV lines respectively; the fluxes (in phot $cm^{-2} s^{-1}$) refer to that pixel in the FCS raster with peak intensity.

and Fe XXV light curves. At lower temperatures significant time-variable emission is found right until the beginning of the subsequent raster image.

In summary, the FCS raster image directly demonstrates the compact nature of the flaring event, while the FCS light curves show the longer decay time-scales for the lower temperature lines.

3.2. The GRS data

3.2.1. *The Instrument*

The SMM Gamma Ray Spectrometer (GRS) consists of seven NaI (Tl) scintillation spectrometers sensitive to γ-rays between 0.28 and 9.28 MeV; pulse height analysis is provided in 476 digital pulse height channels with an energy resolution of $\sim 7\%$ at 0.628 MeV. An auxiliary system of two NaI X-ray detectors gives simultaneous coverage in the hard X-ray band between 10 and 140 keV. The two X-ray detectors are identical except for the entrance filters. Here we consider only data from the detector with an Al–Fe filter giving 50% transmission at ~ 30.8 keV. Pulse height analysis is provided in four energy channels, yielding the energy bands 14–28, 28–56, 56–114, and

https://doi.org/10.1017/S0252921100031997 Published online by Cambridge University Press

114–119 keV. The GRS provides no spatial resolution, and in fact views almost half the sky at any given time. A detailed description of the GRS is given by Forrest *et al.* (1980).

3.2.2. *The Hard X-Ray and γ-Ray Light Curves*

In Figure 6 (left panel) we show the measured light curves in the four energy channels of the hard X-ray detector. The light curves show an interesting double peak structure. In all bands flare onset occurs at 2:55:40 UT, but some 'precursor activity' is definitely present. Towards higher energies the relative strength of the second (later) maximum decreases rapidly and becomes virtually absent at energies above ~ 50 keV; at energies higher than ~ 50 keV only one hard X-ray burst centered on 2:56:10 UT is observed. In the right panel of Figure 6 we show the light curves as measured by the γ-ray spectrometer. The GRS light curves continue the trend observed in the hard X-ray light curves. At γ-ray energies only one burst centered on 2:56:10 UT is visible; at the time of soft X-ray flare maximum, i.e., near 3:00 UT, no substantial γ-ray emission is produced. While we show only the γ-ray light curves up to 2 MeV the γ-ray emission can be detected up to energies of ~ 4 MeV when the signal disappears in the noise.

In summary, the GRS observations demonstrate the very hard spectrum of the first burst, extending into the MeV regime; however, they also show very clearly the existence of a second, presumably purely thermal energy release with a much softer spectrum, that is probably triggered by the first flare event. This complicated double peak structure then explains the slight dip in the Fe XXV emission measure observed at 2:58 UT; while the temperature derived from the Ca XIX and Fe XXV data remains almost unchanged, the second energy release leads to yet another increase in emission measure at temperatures above 10^7 K.

4. The Solar-Stellar Connection: Comparison of the SMM and IPC Observations and Conclusions

With the SMM data we can immediately verify (or falsify) the 'stellar' results as summarised in Section 2. The FCS raster scans can be used directly to measure the extent of the flaring region. Inspection of the FCS images shows that the flare occurred in the active region visible in the lower temperature lines. While it is difficult to tell whether the actual flare emission is extended or not in the lower temperature lines, the flare appears spatially unresolved in the higher temperature lines. Consequently we can only state that the characteristic size scale of the flaring plasma should be less than 14 arc sec, the FCS pixel size, i.e., less than $\sim 10^9$ cm. Thus the IPC measurements overpredict the actual length scale by a factor ~ 3 (or possibly more). Such a disagreement does not come totally unexpectedly considering the multitude of assumptions (as detailed by SHF) that go into a 'stellar' flare size estimates. Also it is important to note that the size estimate depends on the assumed emission measure EM; in order to determine the emission measure SFH assumed the flare plasma to be isothermal at temperatures of ~ 7.2. If low temperature plasma contributes significantly

https://doi.org/10.1017/S0252921100031997 Published online by Cambridge University Press

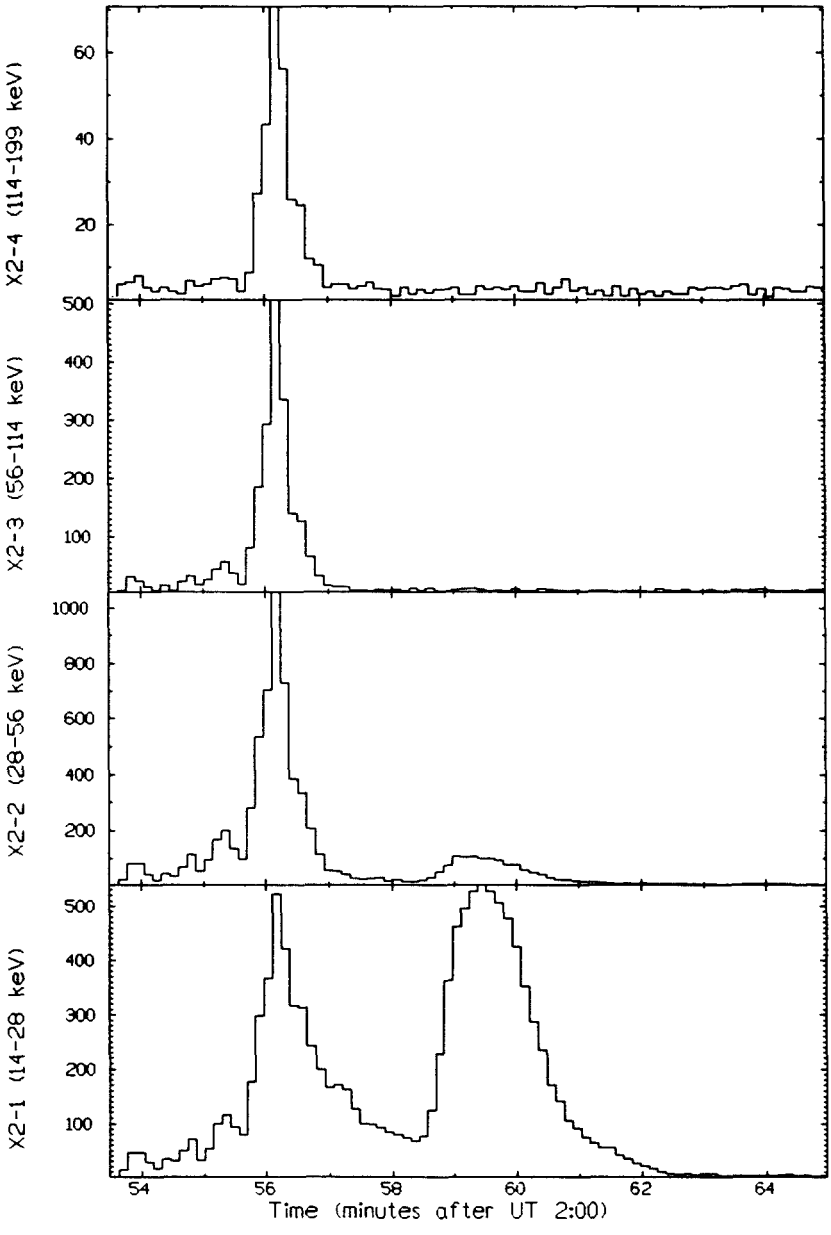

Fig. 6.

to the observed IPC count rate, the emission measure and length scales as derived by SFH will be overestimated as appears to be the case.

A simultaneous FCS and BCS light curve exists in the time interval between 3:02 UT and 3:05. We note, however, that the BCS light curve refers to a 6 arc min total field of view whereas the FCS light curve refers only to the 14 arc sec pixel with

https://doi.org/10.1017/S0252921100031997 Published online by Cambridge University Press

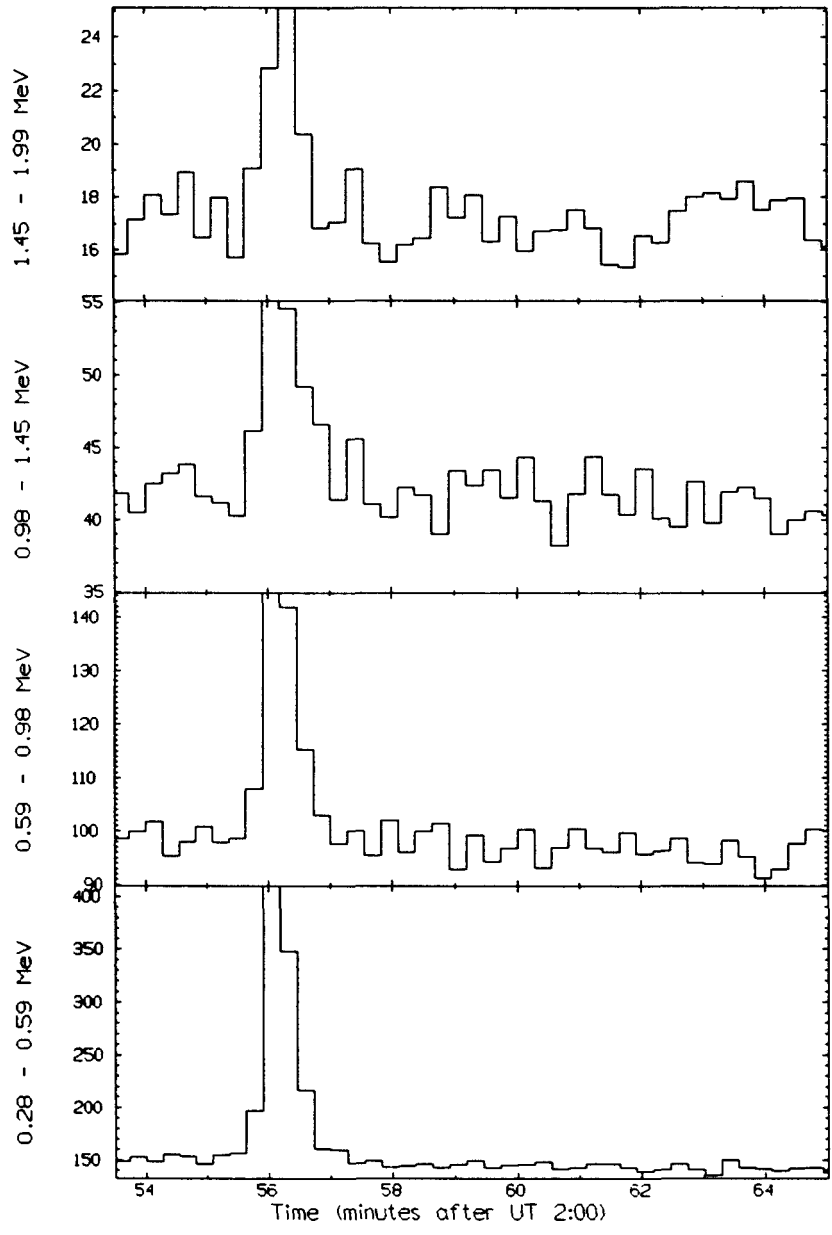

Fig. 6. GRS hard X-ray light curves between 0.14–114 keV (*left panel*) and γ-ray light curves between 0.28 and 2 MeV (*right panel*).

the peak intensity in the previously obtained raster image. A comparison between the raster image taken at 2:56 UT and 3:10 UT shows that the pixel containing the peak emission has moved; hence, the FCS light curves are likely to have missed a significant portion of the flare flux. In fact, because of the cross calibration problem between FCS and BCS fields of view, we were unable to perform a consistent differential emission

https://doi.org/10.1017/S0252921100031997 Published online by Cambridge University Press

measure analysis. However, we find that the FCS low-temperature line fluxes in the first raster image (obtained during the rise phase of the flare) can be reasonably fit by an isothermal source with a mean electron temperature of 5×10^6 K and a volume emission measure of 3×10^{48} cm^{-3}.

Given an isothermal plasma model derived from the BCS spectra (over the full 6 arc min field of view) as well as the FCS model as derived from the raster scan data in the rise phase of the flare we can proceed to estimate how much of the broad band IPC emission can be accounted for by the emission seen with the XRP and compare it to the observed values (cf. Table II). Table II reveals that in the IPC band pass most of the flux comes from the BCS component in the assumed incident spectrum; however, the total predicted IPC count rate falls below the observed IPC count rate in all cases. This fact is of course not unexpected since the emission measure derived from FCS raster scan in the *rising* phase of the flare is likely to be too small for the time immediately after the flare peak. On the other hand, in order to account for *all* of the observed IPC emission with the FCS and BCS components, the FCS emission measure would have to be increased by a factor of 5–10. The same problem is encountered when the emission measures derived from the FCS light curves are used which – as discussed above – are likely to have missed a substantial fraction of the total FCS flare flux. In view of these uncertainties we are not able to determine whether the plasma model as derived from the SMM BCS and FCS data completely accounts for the observed IPC count rate or whether the IPC with its rather soft band pass sees additional low temperature material not visible in the harder FCS and BCS instruments. At any rate, because of the presence of low temperature material (i.e., material cooler than 10^7 K) it is now clear why the emission measures and hence size scales derived from the IPC observations are too large; however, because of our inability to construct an appropriate differential emission measure distribution we are not in a position to provide an improved size estimate.

What can then be learnt from spatially unresolved, low spectral resolution data on stellar flares? We have shown that one of the basic physical parameters of the soft X-ray emissing flaring plasma, i.e., the temperature, can be well estimated. Clearly, the detailed temperature stratification, the dynamics, and the detailed physics of the flaring plasma cannot be addressed observationally in the stellar context. The rather coarse estimates of density and length scale based on the IPC observations are shown to be approximately correct; however, it should be noted that also the XRP data do not allow direct density diagnostics, and therefore in principle the FCS filling factor could be significantly less than unity. The complicated heating structure of the flare event, its double burst structure with an initial nonthermal burst followed by another thermal burst producing extremely hot plasma, is at best hinted at by the soft X-ray data, but can only be revealed by the hard X-ray data; the lack of hard X-ray data is certainly a severe deficiency of the existing body of stellar X-ray flare data.

As far as solar flares are concerned hard X-ray observations are thought to be the key towards an understanding of the flare energetics. In the stellar context hard X-ray observations of flares have never been reported. Although a number of events observed in all-sky surveys of X-ray transients have been identified as huge flares on nearby active

M-dwarfs and somewhat more distant RS CVn systems (cf., Pye and McHardy, 1983; Connors, 1988), the observed emission is very likely to have thermal origin. Scaling solar hard X-ray and γ-ray flares to stellar distances results in mind-boggling observational requirements to detect such events. On the other hand, stellar (soft) X-ray flares are far more energetic than their solar counterparts; the same probably applies also to the impulsive phases of these stellar flares, but it is difficult to extrapolate from the soft X-ray to the hard X-ray and γ-ray regime. Under these circumstances it becomes very important to look for proxy indicators of the impulsive phases of stellar flares and associated hard X-ray and γ-ray emission. On the Sun, microwave bursts are known to correlate extremely well with hard X-ray bursts (cf., Wiehl *et al.*, 1985), and we, therefore, propose that simultaneous microwave and soft X-ray observations may provide (indirect) evidence for the existence of impulsive phases in stellar flares and concurring hard X-ray and γ-ray emission.

Acknowledgements

We thank Dr G. Kanbach for his help with the analysis and interpretation of the GRS data and Dr S. Snowden for help with analysis of scattered solar X-ray radiation.

References

Acton, L. W., Culhane, J. L., Gabriel, A. H., and 21 co-authors: 1980, *Solar Phys.* **65**, 53.
Antonucci, E., Gabriel, A. H., and 7 co-authors: 1982, *Solar Phys.* **78**, 107.
Collura, A., Pasquini, L., and Schmitt, J. H. M. M.: 1988, *Astron. Astrophys.* **205**, 197.
Connors, A.: 1988, Ph.D. Thesis, Univ. of Maryland, NASA report 88–014.
Fink, H. H., Schmitt, J. H. M. M., and Harnden, F. R., Jr.: 1988, *Astron. Astrophys.* **193**, 345.
Forrest, O. J., Chupp, E. L., Ryan, J. M., and 10 co-authors: 1980, *Solar Phys.* **65**, 15.
Gabriel, A. H.: 1972, *Monthly Notices Roy. Astron. Soc.* **160**, 99.
Haisch, B. M.: 1983, in P. B. Byrne and M. Rodonò (eds.), *Activity in Red Dwarf Stars*, Astrophysics and Space Science Library, Vol. 102, p. 255.
Lemen, J. R., Philipps, K. J. H., Cowan, R. D., and Grant, I. P.: 1984, *Astron. Astrophys.* **135**, 313.
Manson, J. E.: 1976, in O. R. White (ed.), *The Solar Output and Its Variation*, Colorado Associated University Press, Boulder.
Pallavicini, R., Monsignori-Fossi, B. C., Landini, M., and Schmitt, J. H. M. M.: 1987, *Astron. Astrophys.* **191**, 109.
Pallavicini, R.: 1987, in E.-H. Schröter and M. Schüssler (eds.), 'Solar and Stellar Flares', *Lecture Notes in Physics* **292**, 98.
Pallavicini, R. and Schmitt, J. H. M. M.: 1988, in W. Hermsen (ed.), *Contribution to COSPAR Advances and Perspectives of X-ray and γ-ray Astronomy*, Helsinki.
Pallavicini, R. *et al.*: 1989, *Astron. Astrophys.* (submitted).
Pye, J. P. and McHardy, I. M.: 1983, *Monthly Notices Roy. Astron. Soc.* **205**, 875.
Schmitt, J. H. M. M., Harnden, F. R., Jr., and Fink, H. H.: 1987, *Astrophys. J.* **322**, 1034.
Strong, K. H. *et al.*: 1986, in *Energetic Phenomena on the Sun*, SMM Flare Workshop, Nasa Conference Publication 2439.
Wiehl, H. J., Batchelor, D. A., Crannell, C. J., Dennis, B. R., Price, P. N., and Magun, A.: 1985, *Solar Phys.* **96**, 339.